

# Gauge Theory Bootstrap: Pion amplitudes revisited

Rafael Cordoba\*

(Dated: September 5, 2024)

In this text we consider the S-Matrix bootstrap of the  $2 - 2$  Pion amplitude as introduced on [2]. We start by considering the general constraints of analyticity, crossing symmetry and unitarity and further restrict the space of amplitudes to match the UV (QCD) and IR (Chiral Perturbation Theory) symmetry information where many results can be found in the literature and are well understood. The crucial realization, for which this work became feasible, is that one can extract information out of these theories using a procedure known as the Form Factor bootstrap to constrain the space of allowed amplitudes matching the IR and UV information.

In this work we keep exploring the framework proposed in [2, 3] by describing the amplitude functions in terms of a discrete basis. This allow us first, to check the consistency of the results and, secondly to efficiently explore the poles of the  $S$ -Matrix. As expected from [3] we found great agreement with experimental/phenomenological data [4–6] on the partial waves of the  $S$ -Matrix and on the poles in the  $S$ -Matrix found in the PDG data [7], where we identified the  $\sigma$ ,  $\rho(770)$  and the  $f_2(1270)$  mesons.

## CONTENTS

I. Introduction	2
II. Discrete basis of functions S-Matrix Bootstrap	4
A. Numerical Setup	5
III. IR and UV constraints	6
A. IR constraint: Chiral Symmetry Breaking	7
B. UV constraint: QCD	8
C. Finite Energy Sum Rules	10
D. Gauge Theory Bootstrap: Numerical Setup	11
IV. Numerical convergences and Results	13
A. Results	16
V. Conclusions	18
References	18

---

\* Laboratoire de Physique de l'Ecole Normale Supérieure, ENS-Université PSL, F-75005 Paris, France ; rf.cordoba@ens-psl.eu

## I. INTRODUCTION

Quantum Field Theory (QFT) is the foundational framework for modern fundamental physics. While perturbative QFT has successfully explained physical phenomena involving weakly interacting quantum fields the case of strongly coupled QFTs remains less understood. Perturbative techniques fall short in this regime, leaving us without a precise, universal mathematical formulation. Remarkably, a substantial volume of non-perturbative results in QFT has emerged recently, thanks to the incredible success of the conformal bootstrap program [8, 9]. Indeed, the use of modern conformal bootstrap techniques, both analytical and computational—which arises from the constraints of symmetries and consistency in a given Conformal Field Theory (CFT), a QFT with a spacetime symmetry extended from the Poincaré group to the conformal group—offers a unified framework to study analytic, strongly coupled, results giving insights for both Lagrangian and non-Lagrangian CFTs.

These techniques are, however, only suitable for theories with conformal symmetry and the extension of these ideas to general relativistic quantum theories transposed into thinking that amplitudes of interactions in a given theory, mainly the S-matrix, might be fully constrained by global symmetries, crossing symmetry, unitarity, and analyticity without relying on an underlying dynamical theory that may or may not be a quantum field theory [10].

In this work we continue the exploration of this bootstrap ideas in the framework of “Bootstrapping Gauge Theories” initiated in [2, 3]. The S-Matrix we consider is that of a  $SU(3)$  gauge theory i.e. QCD with matter content of Left and Right Up and Down quarks interchanged by a  $SU(N_f = 2)_L \times SU(N_f = 2)_R$  global symmetry.

This  $SU(3)$  gauge theory at low energies breaks the global symmetry to a  $SU(2)_V$  global symmetry which comes from Higgsing the global symmetry to its diagonal,

$$SU(2)_L \times SU(2)_R \equiv SU(2)_A \times SU(2)_V \rightarrow SU(2)_V,$$

where  $SU(2)_V$  is the vectorial and  $SU(2)_A$  the axial symmetries. This symmetry breaking is identified by the famous non-vanishing vacuum expectation value (vev) contribution of the quark condensate  $\langle q\bar{q} \rangle$ . At this level, the low energy physics contains the pions  $\pi_a$ , labeled by  $a = 1, 2, 3$  the three generators of the isospin symmetry  $SU(2)$ , as the Goldstone bosons of the symmetry breaking.

Apriori we know the pion-pion scattering,

$$\pi_a(p_1) + \pi_b(p_2) \rightarrow \pi_c(p_3) + \pi_d(p_4), \quad (1)$$

$S$ -Matrix has to be an analytic, crossing symmetric and, unitary function on the physical region. More precisely, if we encode the  $S$ -Matrix information in an analytic function  $A(s, t, u)$  of the Mandelstam variables  $s, t, u$  then, we require the transition function  $T$  ( $S \sim \delta + iT$ ) to respect crossing symmetry as the requirement that  $T$  follows:

$$T_{ab,cd} = A(s, t, u)\delta_{ab}\delta_{cd} + A(t, s, u)\delta_{ac}\delta_{bd} + A(u, t, s)\delta_{ad}\delta_{bc}$$

with  $A(s, t, u) = A(s, u, t)$  and  $a, b, c, d = 1, 2, 3$ . Likewise, to impose the unitarity constraint we consider amplitudes of well-defined isospin ( $I = 0, 1, 2$ ) in the  $s$ -channel:

$$T_{ab,cd} = \frac{1}{3}T^{I=0}\delta_{ab}\delta_{cd} + \frac{1}{2}T^{I=1}(\delta_{ac}\delta_{bd} - \delta_{ad}\delta_{bc}) + \frac{1}{2}T^{I=2}\left(\delta_{ac}\delta_{bd} + \delta_{ad}\delta_{bc} - \frac{2}{3}\delta_{ab}\delta_{cd}\right)$$

with

$$\begin{aligned} T^{I=0}(s, t, u) &= 3A(s, t, u) + A(t, s, u) + A(u, t, s), \\ T^{I=1}(s, t, u) &= A(t, s, u) - A(u, t, s), \\ T^{I=2}(s, t, u) &= A(t, s, u) + A(u, t, s), \end{aligned}$$

where we have decomposed the  $T$  tensor in its trace (isospin-0 rep.), anti-symmetric (isospin-1 rep.) and symmetric traceless (isospin-2 rep.) parts. Now, consider the partial waves given by

$$f_\ell^I(s) = \frac{1}{4} \int_{-1}^{+1} d\mu P_\ell(\mu) T^I(s, t), \quad (2)$$

where  $P_\ell$  are the Legendre polynomials,  $t = -\frac{(s-4)(1-\mu)}{2}$  and,  $u = 4 - t - s$ . To impose unitarity in each partial wave  $S_\ell^I$  we require

$$|S_\ell^I(s)| \leq 1, \forall \ell \in \mathbb{Z}_{\geq 0}, \quad s \in \mathbb{R}_{\geq 4}. \quad (3)$$

Therefore, the  $S$ -Matrix is said to satisfy Unitarity, Crossing, and Analyticity (ACU) provided (3) is satisfied,  $A(s, t, u) = A(s, u, t)$  and,  $T$  is as above. These are minimal assumptions for the  $S$ -Matrix that are believed to be present in most theories, see [10] for details.

To explore this amplitude, one can further parametrize  $A$  using the “Mandelstam representation” for the scattering amplitude as follows: Since the amplitude has a discontinuity on  $s$  and double discontinuity on the  $(s, t)$ ,  $(s, u)$  and  $(t, u)$  (see [1] for details) we can write

$$\begin{aligned} A(s, t, u) = & T_0 + \frac{1}{\pi} \int_4^\infty dx \frac{\sigma_1(x)}{x-s} + \frac{1}{\pi} \int_4^\infty dx \sigma_2(x) \left[ \frac{1}{x-t} + \frac{1}{x-u} \right] \\ & + \frac{1}{\pi^2} \int_4^\infty dx \int_4^\infty dy \frac{\rho_1(x, y)}{x-s} \left[ \frac{1}{y-t} + \frac{1}{y-u} \right] \\ & + \frac{1}{\pi^2} \int_4^\infty dx \int_4^\infty dy \frac{\rho_2(x, y)}{(x-t)(y-u)} \end{aligned} \quad (4)$$

with  $\rho_2(x, y) = \rho_2(y, x)$  to respect the  $u \leftrightarrow t$  symmetry of  $A$  and, were we have set  $m_\pi = 1$  for ease of notation. Therefore, this parametrization allow us to characterize the scattering amplitude (1) by the variables

$$\{T_0, \sigma_{\alpha=1,2}(x), \rho_{\alpha=1,2}(x, y)\} \quad (5)$$

which contain, thus, all the information of the scattering. The subspace (yet infinite dimensional) of parameters (5) satisfying the unitarity condition (3), provided  $\rho_2$  is a symmetric function, defines the space of allowed amplitudes. The **bootstrapped space**, on the other hand, will contain this space as in practice the unitarity condition (3) is imposed only at a finite subset of points  $\{M_i\}_{i=1}^M \subset [4, \infty)$  instead of the entire physical region  $[4, \infty)$ , as we will see shortly.

The crucial realization of [2] is to constrain the space of parameters (5) using the UV and IR information of the theory –where many perturbative results are known–, in addition to the ACU constraints. Pictorially, the bootstrap is illustrated in Figure 1 and we will show in detail how this is done in the following sections.

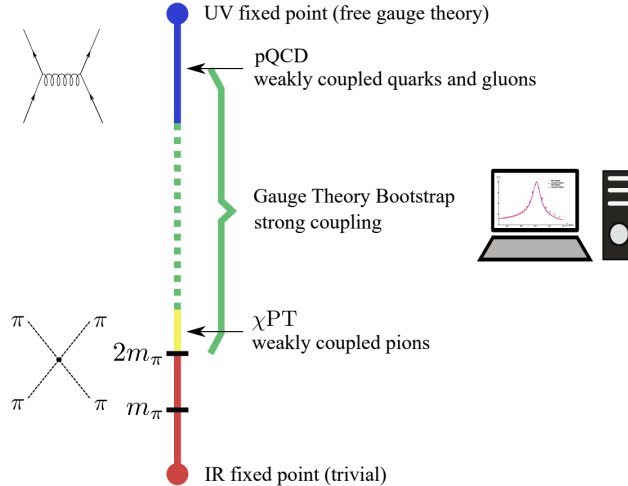


FIG. 1: Gauge Theory Bootstrap. The bootstrap is performed such that it matches the UV and IR information of the standard model and allows to retrieve results in the range where neither is valid. Image retrieved from [3].

As mentioned above, one can reduce the problem to a finite-dimensional basis by performing an **interpolation point method**, in which the variables to be constrained are the functionals of (5) evaluated at a judicious point set  $\{x_i\}_{i=1}^M \in [4, \infty)$  of the physical energies. Then, the amplitudes are characterized by the set of parameters:

$$\{T_0, \sigma_{\alpha=1,2}(x_i), \rho_{\alpha=1,2}(x_i, x_j)\}_{i,j=1}^M \quad (6)$$

that, in turn, allow us to retrieve the  $S$ -Matrix evaluated at each  $\{x_i\}_{i=1}^M$ . Since the constraints are convex, the allowed subspace of gauge theories in which the Pion-Pion theory should lie i.e. the bootstrapped pion space, is then a convex space on the variables of (5), bounded by the variables that extremize the constraints of ACU subject to the

IR and UV linear constraints. These boundary points are special points in the space of allowed amplitudes as they, as we will see later, constitute the amplitudes at which the scattering is dominated by 2-particle pion states and thus, where the non-perturbative results are found. This was further explored in [3], where the theoretical/numerical calculation uses only the pion mass  $m_\pi$ , pion decay constant  $f_\pi$  and the QCD parameters  $N_c = 3, N_f = 2, m_q$  and  $\alpha_s$  to achieve reasonable agreement with experiment and, in particular, key signatures of  $SU(2)_V$  i.e. appearance of the  $\rho(770)$ ,  $f_2(1270)$  and  $\rho(1450)$  resonances are identified.

In this work, instead of redoing the above mentioned method, we employ a discrete basis of functions  $\{\phi_n\}$  by taking

$$\rho(x, y) = \sum_{n_1, n_2} \rho_{n_1 n_2} \phi_{n_1}(x) \phi_{n_2}(y) \quad \& \quad \sigma(x) = \sum_n \sigma_n \phi_n(x). \quad (7)$$

In this case, the space described by (5) is parametrized with

$$\{T_0, \sigma_n^{\alpha=1,2}, \rho_{n,m}^{\alpha=1,2}\}_{n,m=1}^{n_{max}}. \quad (8)$$

for a given cutoff  $n_{max}$  and therefore, an amplitude depends on the evaluation point  $M_i$  and  $n_{max}$  ( $A(s_i, n_{max})$ ).

The purpose of this work is three-fold. First, it allows us to check the consistency of the aforementioned results using a different parametrization from the one explored in [3]. The second is that this set up, which we call the **discrete basis method**, allows us to test the convergences of the input and constraints parameters for the bootstrap which are mainly the number of points evaluated  $s_i = M_i$ , the number of element basis  $n_{max}$ , the number of constraints in the angular momentum  $\ell_{max}$  and, the respective tolerances matching the UV and IR information. This is important as it allows us to identify the set of constraints that contribute meaningful information in the bootstrap constraining the space of parameters (8) as well as choosing the minimal set of parameters for which the amplitude information is contained which, in turn, drastically decreases the time for generating results.

Finally, the discrete basis allows us to have better control than the interpolation method for identifying the resonances of the scattering i.e. the poles of the  $S$ -Matrix. Indeed, although the interpolation point produces an accurate  $S$ -matrix evaluated at each  $M_i$ , which in the discrete basis approach is essentially  $n_{max} \rightarrow \infty$ , for a given number of points  $\{M_i\}_i^M$ , the resolution  $|M_i - M_{i+1}|$  which are, at high energies, very far separated—as we will explain later how this is mapped—is not enough to determine with precision resonances/poles of the  $S$ -Matrix far from the real axis. The discrete basis, in contrast, provides the shape of the amplitude at all points (provided we have generated the associate coefficients and, subject to an error that we later quantify) allowing us to identify more poles of the  $S$ -Matrix. This keeps the bootstrap in a reasonable execution time as the gauge theory bootstrap aims to be a non-perturbative tool for amplitude computations. The result of this is that, in addition to identifying the results of [3], we find the  $\sigma$  a.k.a  $f_0(500)$  meson of which its  $T$ -Matrix pole  $s \in \mathbb{C}$  localizes far from the real axis and thus, it was difficult to find with the methods of [3]. We proceed to elaborate on how this was done.

## II. DISCRETE BASIS OF FUNCTIONS S-MATRIX BOOTSTRAP

Consider the pion-pion scattering of Equation (1). As mentioned above, the  $S$ -Matrix can be parametrized by a function  $A(s, t, u)$  (c.f. Eq. (4)) whose inputs were further parametrize by

$$\rho(x, y) = \sum_{n_1, n_2} \rho_{n_1 n_2} \phi_{n_1}(x) \phi_{n_2}(y), \quad \sigma(x) = \sum_n \sigma_n \phi_n(x),$$

for some coefficients  $\rho_{n,m}$  and  $\sigma_n$ . The simplest functions to use as a basis, for  $n \geq 1$  are

$$\phi_n(x) = \sin(n\varphi), \quad x = \frac{4}{\cos^2 \frac{\varphi}{2}},$$

satisfying  $\phi_n(x \rightarrow 4) \sim \sqrt{x-4}$  and  $\phi_n(x) \simeq x^{-1/2}$  for  $x \rightarrow \infty$ . Since the functionals of Equation (4) are parametrized by a kernel of the form  $1/(x-s)$ , let us define the analytic functions  $\Phi_n(s)$  by:

$$\Phi_n(s) = \frac{1}{\pi} \int_4^\infty dx \frac{\phi_n(x)}{x-s} = z^n - (-1)^n \quad (9)$$

with

$$z = \frac{2 - \sqrt{4-s}}{2 + \sqrt{4-s}}, \quad z(x + i\epsilon) = e^{i\varphi}.$$

We then have general functions, with up to double discontinuities, parametrized by

$$F(s, t, u) = f_0 + \sum_n \sigma_n [\Phi_n(s) + \Phi_n(t) + \Phi_n(u)] + \sum_{nm} \rho_{nm} [\Phi_n(s)\Phi_m(t) + \Phi_n(s)\Phi_m(u) + \Phi_n(t)\Phi_m(u)].$$

For instance, after some algebra, the pion amplitude takes the form

$$h_\ell^I(s) = \frac{\pi}{4} \sqrt{\frac{s-4}{s}} \left\{ f_0 A_\ell^I + \sum_n \left[ A_{\ell n}^I(s) \sigma_n^{(1)} + B_{\ell n}^I(s) \sigma_n^{(2)} \right] + \sum_{nm} \left[ A_{\ell,nm}^I(s) \rho_{nm}^{(1)} + B_{\ell,nm}^I(s) \rho_{nm}^{(2)} \right] \right\}, \quad (10)$$

where we have performed a partial wave decomposition (Equation (2)),

$$h_\ell^I(s) = \pi \sqrt{\frac{s-4}{s}} f_\ell^I(s) \quad \& \quad S_\ell^I(s) = 1 + i h_\ell^I(s) = e^{2i\delta_\ell^I}, \quad (11)$$

and defined the coefficients  $A$  and  $B$  as follows:

$$\begin{aligned} A_\ell^0 &= 2(N+2)\delta_{\ell 0}, & A_\ell^1 &= 0, & A_\ell^2 &= 4\delta_{\ell 0}, \\ A_{\ell,n}^0 &= 2N\delta_{\ell 0}\Phi_n + 2\hat{\Phi}_{n\ell}, & A_{\ell,n}^1 &= 2\hat{\Phi}_{n\ell}, & A_{\ell,n}^2 &= 2\hat{\Phi}_{n\ell}, \\ B_{\ell,n}^0 &= 4\delta_{\ell 0}\Phi_n + 2(N+1)\hat{\Phi}_{n\ell}, & B_{\ell,n}^1 &= -2\hat{\Phi}_{n\ell}, & B_{\ell,n}^2 &= 4\delta_{\ell 0}\Phi_n + 2\hat{\Phi}_{n\ell}, \\ A_{\ell,nm}^0 &= 2N\Phi_n\hat{\Phi}_{m\ell} + 2\Phi_m\hat{\Phi}_{n\ell} + 2\tilde{\Phi}_{nm,\ell}, & A_{\ell,nm}^1 &= 2\Phi_m\hat{\Phi}_{n\ell} + 2\tilde{\Phi}_{nm,\ell}, & A_{\ell,nm}^2 &= 2\Phi_m\hat{\Phi}_{n\ell} + 2\tilde{\Phi}_{nm,\ell}, \\ B_{\ell,nm}^0 &= \Phi_n\hat{\Phi}_{m\ell} + \Phi_m\hat{\Phi}_{n\ell} + N\tilde{\Phi}_{nm,\ell}, & B_{\ell,nm}^1 &= -\Phi_n\hat{\Phi}_{m\ell} - \Phi_m\hat{\Phi}_{n\ell}, & B_{\ell,nm}^2 &= \Phi_n\hat{\Phi}_{m\ell} + \Phi_m\hat{\Phi}_{n\ell}, \end{aligned} \quad (12)$$

only valid for  $I = 0, 2$  and even  $\ell$  or  $I = 1$  and odd  $\ell$ , otherwise all the coefficients vanish due to Bose symmetry being the pion a spinless particle and, were we have defined the partial waves:

$$\hat{\Phi}_{n,\ell}(s) = \int_{-1}^{+1} d\mu P_\ell(\mu) \Phi_n(t) \quad \& \quad \tilde{\Phi}_{nm,\ell}(s) = \int_{-1}^{+1} d\mu P_\ell(\mu) \Phi_n(t) \Phi_m(u).$$

Detailed derivations of this computations can be found in [1]. The pion amplitude thus is characterized by the function  $h_\ell^I(s)$  to which we impose the constraint of unitarity to find the space of allowed functions

$$\{T_0, \sigma_n^{\alpha=1,2}, \rho_{n,m}^{\alpha=1,2}\}_{n,m=1}^{n_{max}}.$$

We proceed to introduce the energy parametrization at which unitarity will be imposed and show the results of this.

### A. Numerical Setup

Since the unitarity condition is evaluated in the physical region  $s > 4$ ,  $4 - s < t < 0$ , following [11], we can map the analyticity region to unit disks for each Mandelstam variable using,

$$z(\nu) = \frac{2 - \sqrt{4 - \nu}}{2 + \sqrt{4 - \nu}}$$

with  $|z(s)| \leq 1$  and the same for  $t$  and  $u$ . Then, in the physical region  $|z(s)| = 1$ ,  $|z(t)| < 1$  and  $|z(u)| < 1$  we can parametrize  $z(s)$  by

$$z(\nu + i\epsilon) = e^{i\phi}, \phi \in (0, \pi), \quad \nu(\phi) = \frac{8}{1 + \cos(\phi)} \quad (13)$$

and, to generate uniform points on this region, we choose uniform angles:

$$\phi_i = \frac{\pi}{M} \left( i - \frac{1}{2} \right), \quad i = 1, 2, \dots, M.$$

Plugging-in in Equation (10), we generate a set of  $S$ -Matrices evaluated at  $s_i := M_i = \nu(\phi_i)$  to which we need to impose the unitarity constraint

$$|S_\ell^I(f_0|_{M_i}, \rho|_{M_i}, \sigma|_{M_i})| \leq 1,$$

for each  $M_i$ ,  $i = 1, \dots, M$ .

Notice that this constraint is a convex constraint which makes the allowed space, parametrized by the functions on (8), a convex space. Therefore, to find the shape of it, it's enough to find the boundary of the space. To do this we can map out the space by maximizing linear functionals with the caveat that, in general, this optimization problem requires a regularization of the upper bound on the norm of the double spectral density  $\rho(x, y)$ . This need arises from the fact that highly oscillating functions added to  $\rho(x, y)$  make little difference in the physical amplitude and putting an upper bound tames these oscillations, see [1] for details.

All in all, we can set  $\|\rho\| < M_{Reg}$  to make the optimization problem feasible and introduce the functional  $f(s = 3)$  as defined in Equation (11). We can therefore project into the first two partial waves of the  $f$  functional,  $f_0^0$  and  $f_1^1$ , which are given by

$$f_\ell^I(3) = \left\{ f_0 A_\ell^I + \sum_n \left[ A_{\ell n}^I(s) \sigma_n^{(1)} + B_{\ell n}^I(s) \sigma_n^{(2)} \right] + \sum_{nm} \left[ A_{\ell, nm}^I(s) \rho_{nm}^{(1)} + B_{\ell, nm}^I(s) \rho_{nm}^{(2)} \right] \right\}_{s=3}$$

and take these as functionals to be maximized. On this two-dimensional space, we can further introduce a variable  $t$  and set the extra constraints  $f_0^0(3) = t \cos \alpha$  and  $f_1^1(3) = t \sin \alpha$  for some fixed  $\alpha$  and  $f_0^0$  and  $f_1^1$  as above. If we maximize  $t$ , the maximum value of  $t$  defines a point at the boundary of the allowed space. Sweeping the values of  $\alpha \in [0, 2\pi]$  gives the shape.

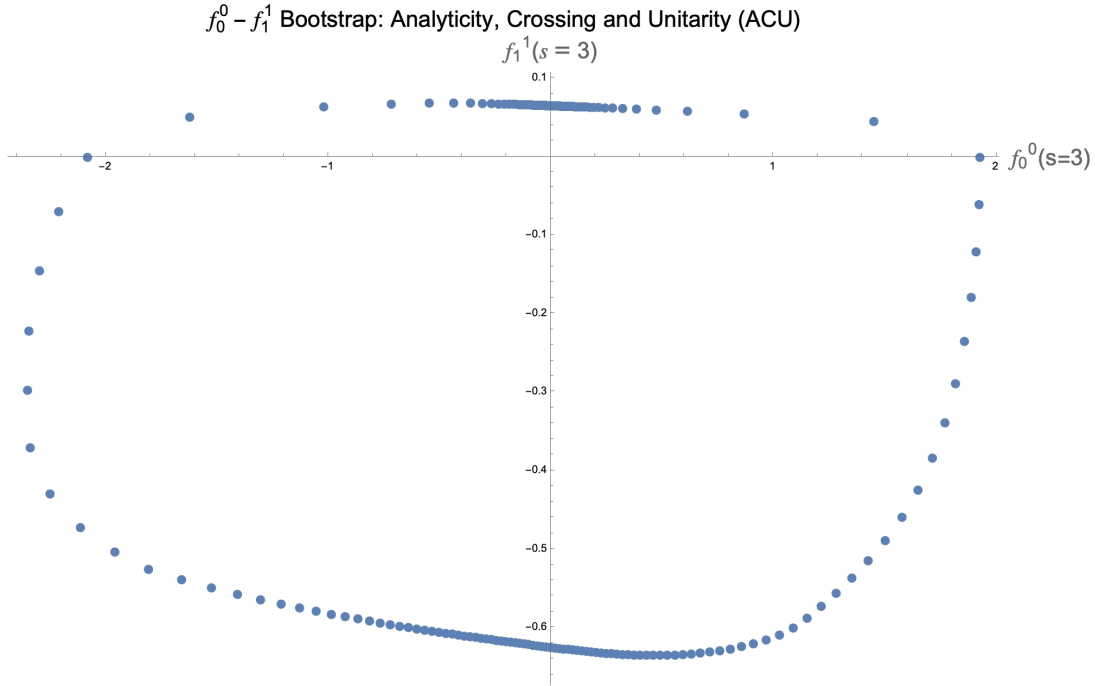


FIG. 2: The space of allowed amplitudes projected onto a plane parameterized by  $f_0^0(s = 3)$  and  $f_1^1(s = 3)$  as a result of pure S-matrix bootstrap with the constraints of analyticity, crossing, and unitarity.  $M = 81$ ,  $I_{max} = 2$ ,  $\ell_{max} = 7$ ,  $n_{max} = 23$ ,  $M_{reg} = 1000$ .

The convex problem is summarized in Table I and the result is shown in Figure 2, where the allowed space (8) under the constraint of ACU is projected on the plane parameterized by  $f_0^0(s = 3)$  and  $f_1^1(s = 3)$  using the discrete basis method. The resulting space is reasonably constrained, in agreement with [2]. The optimization was performed with the MatLab-based modeling system for convex optimization CVX program and the data was generated with Mathematica with precision of 100 significant figures. Mathematica and MatLab code can be found on the Bootstrapping Gauge Theories GitHub repository.

### III. IR AND UV CONSTRAINTS

According to the SM, the pions arise as the bound state of the quark condensate  $q\bar{q}$ . Indeed, at low energy, after the vev of the quark condensate has become non-zero i.e. the global Left and Right ( $SU(2)_L \times SU(2)_R$ ) symmetry

TABLE I: Bootstrap Analyticity, Crossing, Unitarity: On the left the variables of the convex optimization are described with their respective constraint. On the right, the functionals (depending on these variables) and their constraint are shown.

Variables	Constraint	Functionals	Constraint
$f_0$	-	$f_0^0(3)$	Equal to $t \cos \alpha$
$\rho_{n,m}^{(1)}$	$< M_{Reg}$	$f_1^1(3)$	Equal to $t \sin \alpha$
$\rho_{n,m}^{(2)}$	$< M_{Reg}$ , Symmetric	$ S_\ell^I(M_i) $	$< 1$
$\sigma_n^{(1)}$	-		
$\sigma_m^{(2)}$	-		
$t$	Maximize		

has been broken to a diagonal  $SU(2)_V$ , the pions arise as the Goldstone bosons of this symmetry breaking. This weakly interacting theory is well described by the so-called ‘‘Chiral Lagrangian’’ Effective Field Theory (EFT),

$$\mathcal{L} = \frac{f_\pi^2}{4} \left\{ \text{Tr} (\partial_\mu U \partial^\mu U^\dagger) + m_\pi^2 \text{Tr} (U + U^\dagger) \right\},$$

where we have introduced the mass of the Pions  $m_\pi$ , the pion decay constant  $f_\pi$  and

$$U(x) := e^{i \frac{\tau^a \pi_a(x)}{f_\pi}},$$

where the fundamental degrees of freedom are the pions  $\pi_a$  labelled by each index of the  $SU(2)$  generators  $\tau_a$  (3 indices). We compute the interacting terms to each order by expanding the  $U$  exponential. For instance, to second order, we have the kinetic and mass terms:

$$\mathcal{L}_2^{2\pi} = \frac{1}{2} \partial_\mu \pi_a \partial^\mu \pi_a - \frac{1}{2} m_\pi^2 \pi_a \pi_a.$$

Notice, however, that this EFT at tree level is only valid at lowest order in the energy expansion. At the next order, one encounters higher order energy terms and, one-loop diagrams which, in turn, introduces a large amount of parameters that cannot be retrieved from gauge theories or symmetry considerations.

### A. IR constraint: Chiral Symmetry Breaking

Using this Lagrangian, the amplitude of Equation (1) at tree level is computed to be:

$$A(s, t, u) = \frac{s - m_\pi^2}{8\pi^2 f_\pi^2}.$$

One can then compute each partial wave  $f_l^I$  giving

$$f_0^0(s) = \frac{2}{\pi} \frac{2s - m_\pi^2}{32\pi f_\pi^2}, \quad f_1^1(s) = \frac{2}{\pi} \frac{s - 4m_\pi^2}{96\pi f_\pi^2}, \quad f_0^2(s) = \frac{2}{\pi} \frac{2m_\pi^2 - s}{32\pi f_\pi^2}.$$

Since we set the scale  $m_\pi = 1$ , we can impose this linear model without putting the extra information of  $f_\pi$  by taking the ratio

$$R_{21}^X(s) = \frac{f_0^2(s)}{f_1^1(s)} = \frac{3(2-s)}{s-4}, \quad R_{01}^X(s) = \frac{f_0^0(s)}{f_1^1(s)} = \frac{3(2s-1)}{s-4}. \quad (14)$$

The signature of the chiral symmetry breaking therefore can be quantified as the constraint on how close the Chiral Lagrangian model –also called the Weinberg model– ratios is from our theory. This is therefore encoded in the constraint

$$\|R^{\text{boot}}(s_j) - \underbrace{R^X(s_j)}_{\chi_{\text{Tree}}} \| \leq \varepsilon_{CSB}, \quad s_j \in (0, 4) \quad (15)$$

where  $R^{\text{boot}}(s_j)$  are the bootstrap value we are constraining,  $R^\chi(s_j)$  are the Chiral Lagrangian tree level value of (14), which we call  $\chi_{\text{Tree}}$  and, we evaluate at  $s_j = j/2$ ,  $j = 0, 1, \dots, 4$ . The result of adding to the ACU bootstrap (Table I) the CSB constraint (15) is showed in Figure 3 where the tree level Weinberg model is showed by the blue dotted line and, each point on the line represents a value of  $f_\pi$ . We highlight the physical  $f_\pi = 92\text{MeV}$  in a black triangle and, for the bootstrapped space, we take different tolerances  $\epsilon_{CSB}$  of the chiral symmetry breaking. The two bootstrapped points closest to the physical  $f_\pi$  value, each one above and below the hyperplane separated by the Weinberg model line, are enclosed in grey and red ovals and we call them “Up” and “Down” points respectively. We remark that the information of the Pion decay  $f_\pi$  is only used to find the tolerance  $\epsilon_{CSB}$  at which the boundary of the allowed space is closest to the point.

From the graph we observe that the space of Figure 2 is considerably constrained from a scale  $O(1)$  to a scale of  $O(10^{-3})$ . At this point it is worth mentioning that each point of Figure 3 represent a choice of extremal set of param-

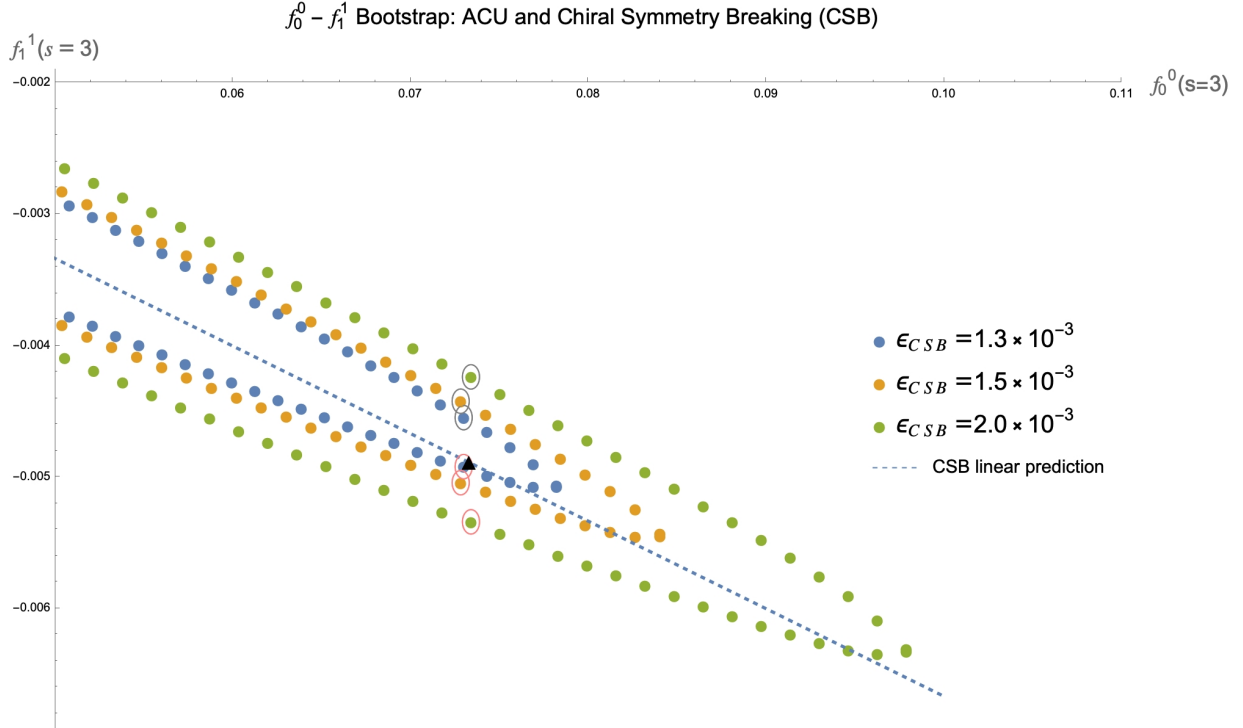


FIG. 3: Space of allowed theories satisfying ACU and the chiral symmetry breaking constrain with an  $\epsilon_{CSB}$  tolerance. The physical point,  $f_\pi = 92\text{MeV}$  is shown as the triangle black mark. The points enclosed in grey and red are the closest points, in the perimeter of the allowed space, to the physical point, above and below the hyperplane cutted by  $f_1^1(3) = -\frac{1}{15}f_0^0(3)$  from the linear model respectively.  $M = 81$ ,  $n_{\max} = 23$ ,  $\ell_{\max} = 7$ .

eters (8) which, in turn, represents an amplitude  $A(s, t, u)$ . The bootstrap amplitude thus gives us a computational tool to compare these amplitudes with experiments. From now on, for a given bootstrapped space we always choose the bootstrapped  $S$ -Matrix of the Up and Down points as they are the closest points to the physical value.

## B. UV constraint: QCD

In this section we introduce the form factor bootstrap which was developed as a way to introduce form factors information of the UV fixed point, in this case QCD, into the low energy bootstrap. We begin by considering the currents on the  $S0$  and  $P1$  waves

$$\begin{aligned} S0 &: j_S(x) = m_q(\bar{u}u + \bar{d}d) \\ P1 &: j_V^\mu(x) = \frac{1}{2}(\bar{u}\gamma^\mu u - \bar{d}\gamma^\mu d) \end{aligned}$$

with standard  $u$  and  $d$  quark notation. Noticing that the vector current is conserved,  $\partial_\mu j_V^\mu = 0$ , and using Lorentz symmetry, we can write the pion form factor as

$$\begin{aligned}\langle_{\text{out}} \pi^+(p_2) | j_S(x) | \pi^+(p_1) \rangle_{\text{in}} &= e^{i(p_1-p_2)x} F_0(t) \\ \langle_{\text{out}} \pi^+(p_2) | j_V^\mu(x) | \pi^+(p_1) \rangle_{\text{in}} &= e^{i(p_1-p_2)x} (p_1^\mu + p_2^\mu) F_1(t)\end{aligned}$$

where  $t = (p_1 - p_2)^2$  and,  $F_0$  and  $F_1$  are the form factors for the currents on  $S0$  and  $P1$  waves respectively. For states of fixed angular momentum and isospin, we find

$$\langle_{\text{out}} I = 0, I_3 = 0; P\ell\sigma | j_S(0) | 0 \rangle = \mathcal{F}_0^0(s) \delta_{\ell 0} \delta_{\sigma 0}$$

$$\langle_{\text{out}} I = 1, I_3 = 0; P\ell\sigma | j_{V,\sigma'}(0) | 0 \rangle = \mathcal{F}_1^1(s) \delta_{\ell 1} \delta_{\sigma \sigma'},$$

with

$$\mathcal{F}_0^0(s) = \frac{\sqrt{6\pi}}{16\pi^3} \frac{1}{s^{\frac{1}{4}}} \left( \frac{s-4}{4} \right)^{\frac{1}{4}} F_0(s), \quad \mathcal{F}_1^1(s) = \sqrt{\frac{4\pi}{3}} \frac{1}{8\pi^3} \frac{1}{s^{\frac{1}{4}}} \left( \frac{s-4}{4} \right)^{\frac{3}{4}} F_1(s) \quad (16)$$

and we used the orthogonality of the Gegenbauer polynomials, see [12] for details. Now, as shown in [2], one can find  $F_i(0) = 1$ , and, since the form factors are analytic functions of  $s$  with a cut on the real axis for  $s > 4$ , we can write a subtracted dispersion relation

$$F_\ell(s) = 1 + \frac{1}{\pi} \int_4^\infty dx \left( \frac{1}{x-s} - \frac{1}{x} \right) \text{Im}F_\ell(x).$$

Introducing the parametrization of the imaginary part of the form factor in terms of our discrete basis,  $\text{Im}F_\ell(x) = \sum \text{Im}F_\ell^n \phi_n(x)$ , we can use the definition of  $\Phi_n$  (c.f. Eq. (9)) on the partial wave expansion to find the relation:

$$F_\ell(s) = 1 + \sum_n z^n \text{Im}F_\ell^n = 1 + \sum_n e^{in\varphi} \text{Im}F_\ell^n,$$

where  $s = \nu(\varphi)$  as defined in Equation (13). Finally, we can find the spectral density by introducing the vacuum polarizations

$$\Pi_1^1(s) \delta_{\sigma' \sigma} = i \int \frac{d^4x}{(2\pi)^4} e^{iPx} \langle 0 | \hat{T} \left\{ j_{\sigma'}^\dagger(x) j_\sigma(0) \right\} | 0 \rangle$$

which are analytic functions of  $s$  with a cut on the real axis for  $s > 4$ . The spectral density, *i.e.*, discontinuity along the cut is given by

$$\rho_\ell^I(s) = 2 \text{Im} \Pi_\ell^I(x + i\epsilon) = \int \frac{d^4x}{(2\pi)^4} e^{iPx} \langle 0 | j_\ell^{I\dagger}(x) j_\ell^I(0) | 0 \rangle$$

which, on the discrete basis  $\phi_n$ , then we can write as

$$\rho_\ell^I(s) = \sum_n \phi_n(s) \rho_\ell^{I,n} = \sum_n \sin(n\varphi) \rho_\ell^{I,n},$$

where  $\rho_\ell^{I,n}$  are the coefficients we want to bootstrap. Now, to couple the form factor and the spectral density to the bootstrap, consider the two pion particle states  $|_{\text{out}}\rangle_{P,I,\ell}$  and  $|_{\text{in}}\rangle_{P,I,\ell}$  and, the state

$$\mathcal{O}_{P,I,\ell} | 0 \rangle, \quad \mathcal{O}_{P,I,\ell} = \int \frac{d^4x}{(2\pi)^4} e^{-iPx} j_l^i(x).$$

The key realization of [12] is to consider the matrix of inner products on these states known as the “B-Matrix”. In this case one can show that

$$B := \begin{pmatrix} 1 & S_\ell^I(s) & \mathcal{F}_\ell^I \\ S_\ell^{I*}(s) & 1 & \mathcal{F}_\ell^{I*} \\ \mathcal{F}_\ell^{I*} & \mathcal{F}_\ell^I & \rho_\ell^I(s) \end{pmatrix} \succeq 0, \quad (17)$$

where we have chosen the ordered basis

$$B : \{|\text{out}\rangle_{P,I,\ell}, \quad |\text{in}\rangle_{P,I,\ell} \quad \mathcal{O}_{P,I,\ell}|0\rangle\} \rightarrow \{|\text{out}\rangle_{P',I,\ell}, \quad |\text{in}\rangle_{P',I,\ell} \quad \mathcal{O}_{P',I,\ell}|0\rangle\}.$$

The form factors and spectral density are thus coupled with the amplitudes through the positive semi-definite matrix constraint which, in turn, extends the functional bootstrap variables to

$$\{f_0, \sigma_{\alpha=1,2}(x), \rho_{\alpha=1,2}(x,y), \text{Im}F_\ell(x), \rho_\ell^I(x)\}. \quad (18)$$

This is known as the **form-factor bootstrap**. Notice that the positive semi-definite condition of the  $B$ -Matrix implies that its leading principal minors are positive. In particular, this restricts  $\rho \geq |\mathcal{F}|^2$  which means that the spectral density is saturated by two pion states. Therefore, optimization on these points gives extremal amplitudes where non-perturbative computations of the amplitudes are found. At high energy, instead, the constraint is saturated by multiparticle states and the form factors are much lower than this bound.

### C. Finite Energy Sum Rules

In the limit of large energy, at leading order in  $s \rightarrow \infty$  and leading order in QCD perturbation theory, the current correlations behave as:

$$\Pi_0^0(s) \simeq \frac{N_c N_f m_q^2}{(2\pi)^4} \frac{(-s)}{8\pi^2} \ln\left(-\frac{s}{\mu^2}\right), \quad \Pi_1^1(s) \simeq \frac{N_c}{(2\pi)^4} \frac{(-s)}{24\pi^2} \ln\left(-\frac{s}{\mu^2}\right) \quad (19)$$

which allows to introduce  $N_c$  in the low energy theory and should give a reasonable initial approximation for the bootstrap. Here,  $\mu$  is the renormalization scale that we can take as  $\mu^2 = s_0$ , the scale at which we later match with the bootstrap. The previous result just computes the current correlation in the high energy vacuum using a quark loop and can be interpreted as keeping the component proportional to the identity in the current OPE:

$$T\{j(x)j(0)\} = C_1(x)1 + \sum_{\mathcal{O}} C_{\mathcal{O}}(x) \mathcal{O}(0).$$

In the symmetry broken vacuum, however, other operators contribute to the QCD result, and we get the SVZ expansion

$$\langle 0|T\{j(x)j(0)\}|0\rangle = C_1(x) + C_{\bar{q}q}(x) \langle 0|j_S(0)|0\rangle + C_{G^2}(x) \langle 0|\frac{\alpha_s}{\pi} G_{\mu\nu}^a G^{a\mu\nu}|0\rangle + \dots$$

where computations in the  $C_1(x)$  term can all be computed using perturbation theory as they come from weakly coupled QCD and, all the other terms are not accessible through perturbation theory, however, it can be retrieved from lattice computations or, as further bootstrap variables. Here we consider they are suppressed by  $\alpha_s$ , but higher precision computations require them. The inclusion of these contributions in the bootstrap is done through a procedure called Finite Energy Sum Rules (FESR).

For the FESR, consider  $s^n \Pi_0^0(s)$ ,  $n \in \mathbb{Z}_{\geq 0}$  and  $s^n \Pi_1^1(s)$ ,  $n \in \mathbb{Z}_{\geq -1}$  where the value  $n = -1$  is allowed since  $\Pi_1^1(s)$  has a zero at  $s = 0$  in the way we defined it. We set  $s_0 = \mu^2$  the high energy scale and, using a renormalization point of view, it can be thought off as the cut off of the theory where beyond  $s_0$  the QCD degrees of freedom are not relevant anymore. Integrating  $s^n \Pi_0^0(s)$  on the region below  $s_0$ , the contour integral has a contribution from the (large) circle at  $|s| = s_0$  and one from the jump across the cut. All in all, we obtain

$$\int_4^{s_0} \rho(x) x^n dx = -s_0^{n+1} \int_0^{2\pi} e^{i(n+1)\varphi} \Pi(s_0 e^{i\varphi}) d\varphi$$

and, using the expansion in the RHS of Equation (19) and, that for  $n \in \mathbb{Z}$

$$\int_0^{2\pi} e^{in\varphi} \ln(e^{i\varphi}) = \frac{2\pi}{n}, \quad n \neq 0, \quad \int_0^{2\pi} e^{in\varphi} d\varphi = 2\pi \delta_n,$$

we find

$$\begin{aligned} \int_4^{s_0} \rho_0^0(x) x^n dx &= \frac{s_0^{n+1} N_f m_q^2}{(2\pi)^4} \left\{ \frac{3s_0}{4\pi(n+2)} \left( 1 + \frac{13}{3} \frac{\alpha_s}{\pi} \right) \right. \\ &\quad \left. + \delta_n \frac{\pi}{4s_0} \langle \frac{\alpha_s}{\pi} G^2 \rangle + \delta_n \frac{3\pi}{s_0} \langle j_S \rangle + \dots \right\}, \quad n \geq 0, \\ \int_4^{s_0} \rho_1^1(x) x^n dx &= - \frac{s_0^{n+1}}{(2\pi)^4} \frac{1}{2} \left\{ - \frac{s_0}{2\pi(n+2)} \left( 1 + \frac{\alpha_s}{\pi} \right) \right. \\ &\quad \left. + \delta_n \frac{\pi}{6s_0} \langle \frac{\alpha_s}{\pi} G^2 \rangle + \delta_n \frac{2\pi}{s_0} \langle j_S \rangle + \dots \right\}, \quad n \geq -1. \end{aligned} \quad (20)$$

Equations (20), when discretized the integral, are linear constraints on the spectral density  $\rho_\ell^I(x)$  that incorporate information on the UV theory which we impose on the bootstrap. In this paper we impose  $n = 0, 1, 2$  for the  $S0$  wave and  $n = -1, 0, 1$  for the  $P1$  wave,

$$\left| \int_4^{s_0} \rho^{boot}(x) x^n dx - \underbrace{\int_4^{s_0} \rho(x) x^n dx}_{FESR} \right| < \varepsilon_{SVZ}, \quad (21)$$

where we have suppressed the isospin and angular momentum indices and,  $\rho_\ell^{boot,I}(x)$  is the bootstrap value to be optimized and  $FESR$  is the one-loop QCD value of Equation (20). Notice that, as said above, the  $C_{G_2}$ ,  $C_{q\bar{q}}$  and beyond terms are difficult to compute but fortunately they are suppressed with  $\alpha_s$ . We can therefore, as we do in this paper, for a tolerance of  $\varepsilon_{SVZ}$  high enough, use only the  $C_1$  terms so that higher order terms are within the range of tolerance.

Finally, for the regions  $s > s_0$ , we need the high energy behaviors of the form factor from QCD. Using a QCD/parton model one can get that the pion form factors

$$F_\pi(s) \simeq - \frac{16\pi\alpha_s(s) f_\pi^2}{s}$$

for  $s \rightarrow -\infty$  which was found for the electromagnetic form factor. This means that as  $s \rightarrow -\infty$  then the form factor tends to zero so that, at high energies which we call  $s_0$  and quarks are essentially free, we set the constraint

$$|\mathcal{F}^{boot}(s > s_0)| \leq \varepsilon_{FF} \quad (22)$$

on the bootstrap variables  $\mathcal{F}^{boot}$  as defined in Equation (16), where we have suppressed the isospin and angular momentum labels. All in all, the bootstrap variables of the ‘‘Gauge Theory Bootstrap’’ are

$$\{f_0, \sigma_{\alpha=1,2}^n, \rho_{n,m}^{\alpha=1,2}, \text{Im}F_\ell^n, \rho_\ell^{n,I}\}_{n,m=1}^{n_{max}}, \quad (23)$$

and the bootstrap is schematically showed in Table II.

#### D. Gauge Theory Bootstrap: Numerical Setup

Let us summarize how the method manages to incorporate gauge theory information into the low energy bootstrap. After the ACU constraint has been implemented, we introduce the form factors and spectral densities to match the constraints below and above  $s_0$ . Above  $s_0$ , the asymptotic form of the vacuum polarizations  $\Pi_\ell^I(s)$  for large  $s$  is obtained from perturbative QCD, Equation (20), while above, the information is given by the vacuum condensates (22). The low energy CSB is incorporated through the Weinberg model, Equation (15). The Finite Energy Sum Rules relate that behavior to integrals of the spectral density in the intermediate energy region. In that region the spectral density is saturated by two pion states and therefore agrees with the modulus squared of the form factor (17). By analyticity, the modulus of the form factor determines its phase. Since we also expect unitarity to be saturated, by Watson’s theorem, the phase of the form-factor and partial waves are the same. In that way, the information from pQCD enters the bootstrap [3]. The parameters we set in the computation are:

$$s_0 = (2\text{GeV})^2, \quad m_\pi = 1, \quad \alpha(2\text{GeV}) = 0.3145887440, \quad m_u(2\text{GeV}) = 3.6m_\pi, \quad m_d = 6.5m_\pi, \quad (24)$$

TABLE II: Gauge Theory Bootstrap: On the left the variables of the convex optimization are described with their respective constraint. On the right, the functionals (depending on these variables) and their constraint are shown. The \* constraint is the positive definite condition of the  $B$ -Matrix from Equation (17).

Variables	Constraint	Functionals	Constraint
$f_0$	-	$f_0^0(3)$	Equal to $t \cos \alpha$
$\rho_{n,m}^{(1)}$	$< M_{Reg}$	$f_1^1(3)$	Equal to $t \sin \alpha$
$\rho_{n,m}^{(2)}$	$< M_{Reg}$ , Symmetric	$ S_\ell^I(s_i) $	$< 1, *$
$\sigma_n^{(1)}$	-	$ R^\chi(s_i) - \chi_{Tree} $	$< \varepsilon_{CSB}$
$\sigma_m^{(2)}$	-	$ \int_4^{s_0} \rho(x) x^n dx - FESR $	$< \varepsilon_{SVZ}$
$t$	Maximize	$ \mathcal{F}(s_i > s_0) $	$< \varepsilon_{FF}$
$ImF_\ell^n$	-	$\mathcal{F}(s_i)$	*
$\rho_\ell^{n,I}$	-	$\rho(s_i)$	*

where, as said earlier, we set  $m_\pi = 1$ . Since the FESR depend on  $s_0$ , now we can write the numerical estimates of  $FESR$  for  $s_0 = 2$  GeV to be:

$$FESR_0^0 := \frac{1}{s_0^{n+2}} \int_4^{s_0} \rho_0^0(x) x^n dx \simeq 3.09 \times 10^{-8} \left\{ \frac{27.38}{n+2} + 0.61 \delta_n + \dots \right\}, \quad (25)$$

$$FESR_1^1 := \frac{1}{s_0^{n+2}} \int_4^{s_0} \rho_1^1(x) x^n dx \simeq -4.34 \times 10^{-6} \left\{ -\frac{13.26}{n+2} + 0.41 \delta_n + \dots \right\}. \quad (26)$$

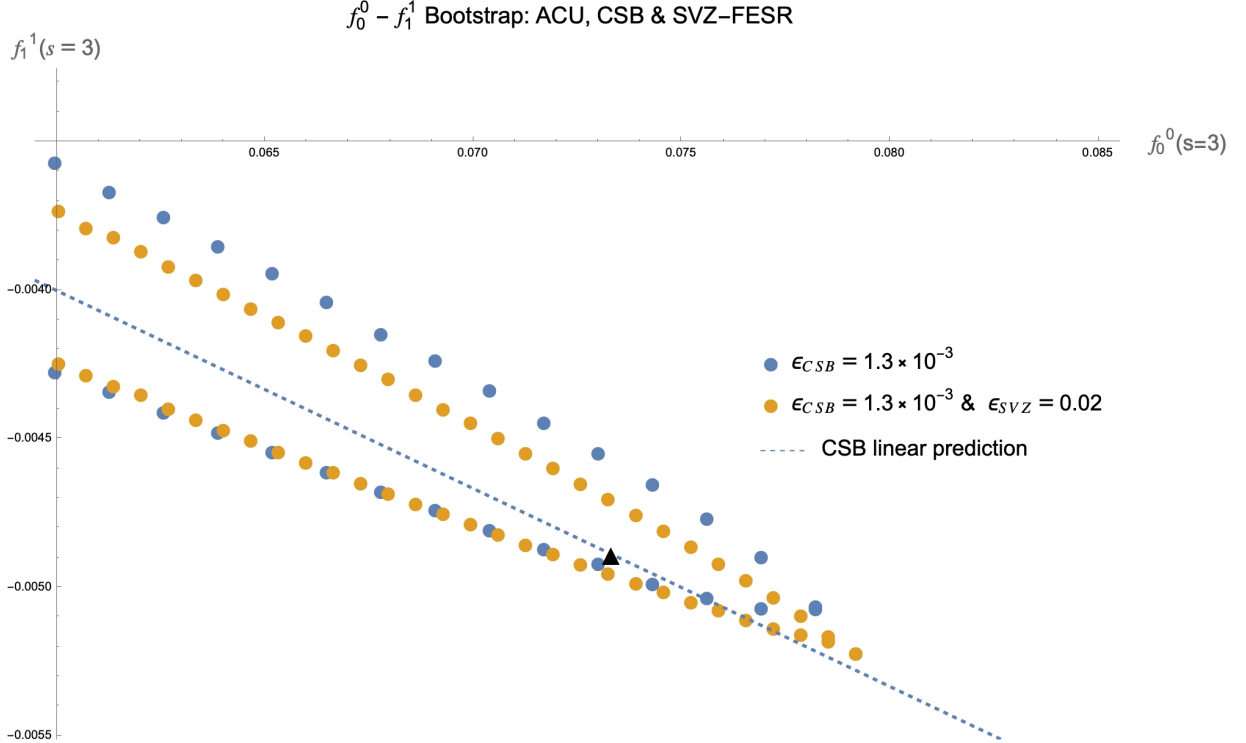


FIG. 4: Space of allowed theories satisfying ACU, CSB and the sum rules constraints. The physical point,  $f_\pi = 92\text{MeV}$  is signaled with the blue dot. The grey and light grey points show the closest points in the perimeter of the allowed space in the plane cutted by  $f_1^1 = -\frac{1}{15}f_0^0$  from the linear model.

In the bootstrap, we bound the spectral density  $\rho_\ell^I(s)$  by approximating the integral with the evaluation at  $\{s_i\}_{i=1}^M$ ,

$$\int_4^{s_0} dx \rho(x) x^n \rightarrow \frac{\pi}{M} \sum_{i=1}^{M'} \left( \frac{ds}{d\phi} \right)_i s_i^n \rho_i,$$

where we have defined  $\rho_i := \rho(s_i)$ ,  $M'$  such that for all  $i > M'$  then  $s_i > s_0$  and, suppressed the quantum numbers for ease of notation. Then we impose the SVZ constraints:

$$\left\| \frac{\pi}{M} \sum_{i=1}^{M'} \left( \frac{ds}{d\phi} \right)_i s_i^n \rho_i - \text{FESR} \right\| \leq \varepsilon_{\text{SVZ}},$$

and, the form factor constraints:

$$\|\mathcal{F}_0(s_i)\|^2 \lesssim \varepsilon_{FF}, \quad \|\mathcal{F}_1(s_i)\|^2 \lesssim \varepsilon_{FF}, \quad s_i > s_0.$$

Implementing these constraints further reduces the space to incorporate the information in the bootstrap as shown in Figure 4, in accordance with [2]. We observe that putting the sum rules and form factor behavior pushes in the upper part of the shape while the lower part does not change too much. The information on the Up and Down points, however, does change on both of them to resemble the experimental/phenomenological predictions as shown in the results section. The constraints of ACU, CSB, FESR and form factor asymptotic had implemented the proposed gauge theory bootstrap, but we have some parameters, mainly  $M$ ,  $n_{max}$ , number of constraints in angular momentum  $\ell$ , etc. to test the numerical convergences and their information contribution to the bootstrap, we proceed to see this.

#### IV. NUMERICAL CONVERGENCES AND RESULTS

Recall that each partial wave is parametrized by the functions shown in (18). Under the discrete basis of functions, the amplitudes  $S_\ell^I(s)$ , the form factors  $F_i(s)$  and the spectral density  $\rho_i$  are characterized by the functions

$$\{f_0, \sigma_{\alpha=1,2}^n, \rho_{n,m}^{\alpha=1,2}, \text{Im}F_\ell^n, \rho_\ell^{n,I}\}_{n,m=1}^{n_{max}} \quad (27)$$

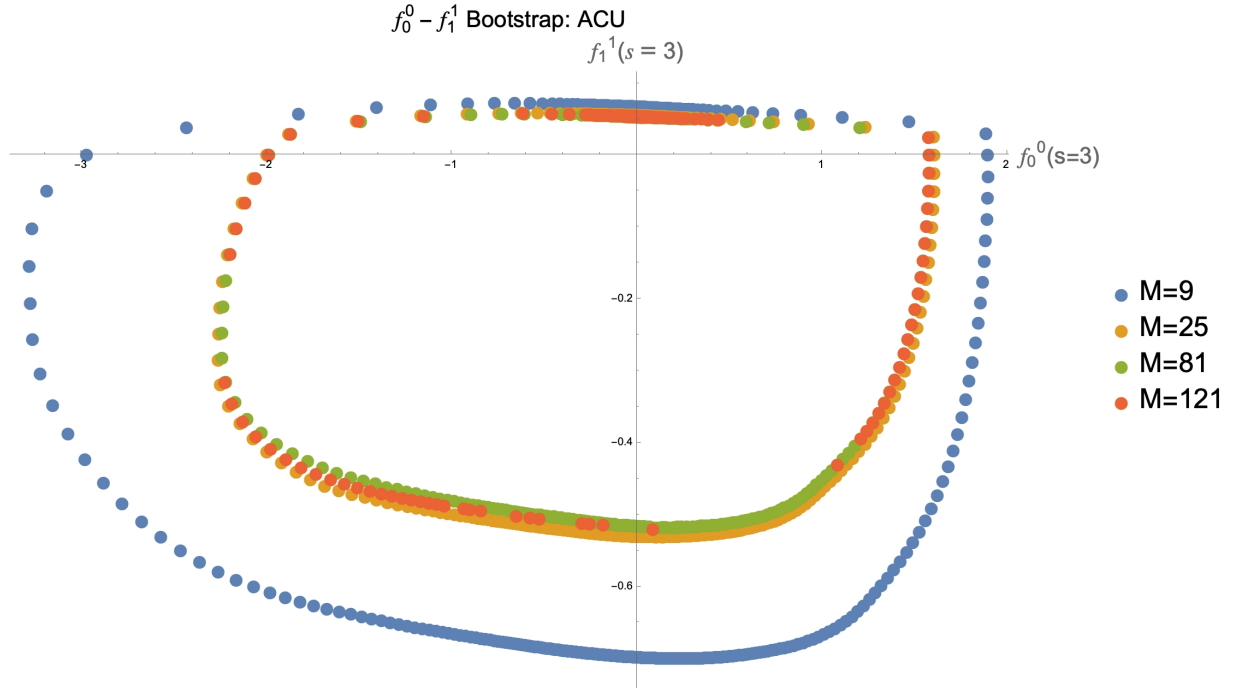


FIG. 5:  $M$  convergence comparison.  $n_{max} = 11$ ,  $\ell_{max} = 7$ .

and, some coefficients  $A$  and  $B$  each of which depend on the points we are evaluating  $\{M_i\}_{i=1}^M$  and wave numbers  $\ell$  and  $I$ , as shown in Equation (10). The functions of (27) are thus the variables we are going to bootstrap by imposing the constraints as shown in Table II and, on the other hand, we have computed the coefficients  $A$  and  $B$  with 100 significant figures with the help of **Mathematica** to compute the functionals of Table II. We show the convergence of  $M$ ,  $n_{max}$ , and,  $l_{max}$  parameters in Figures 5, 6 and, 8 and, since it is often useful to use the phase shift  $\delta_\ell^I$ , recall  $S_\ell^I(s) \equiv \eta_\ell^I(s)e^{2i\delta_\ell^I(s)}$  where  $\eta$  is the so-called elasticity of the amplitude, we have plotted the first six phase shifts to test the convergence on  $n_{max}$  on Figure 7.

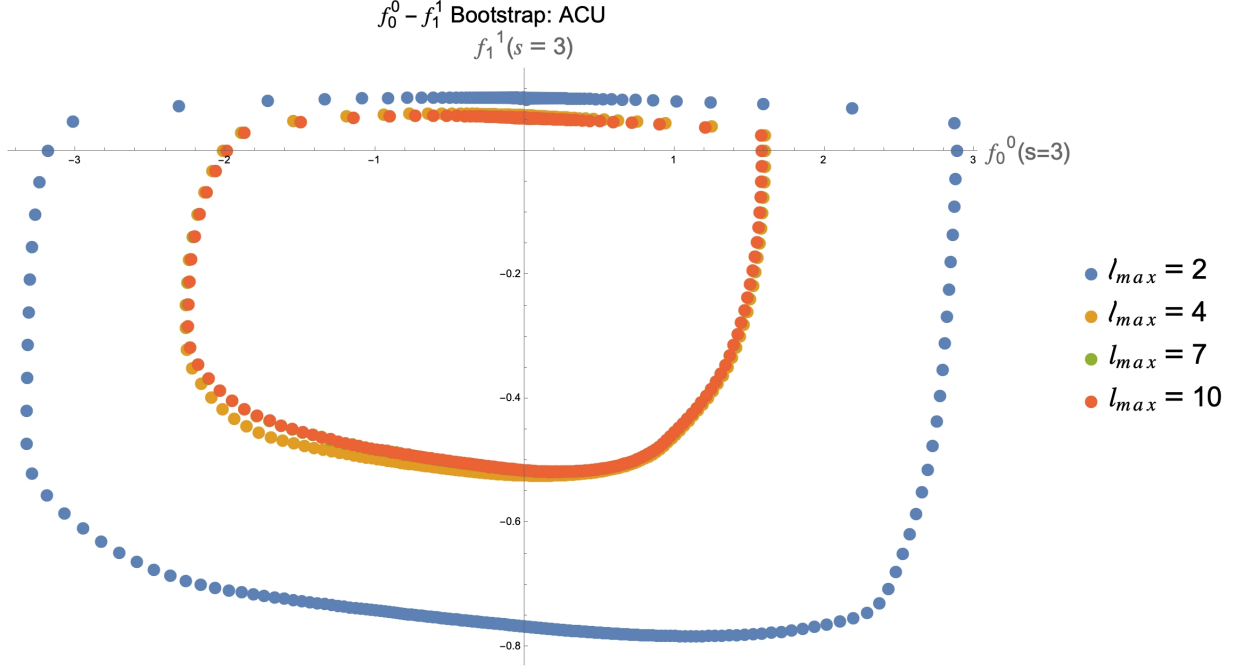


FIG. 6:  $l_{max}$  convergence comparison.  $M = 49$ ,  $n_{max} = 11$ .

On Figure 5 we observe that after  $M > 25$  the space stabilizes into a region. For  $M = 25$ , in the way we have generated the evaluation points, there are only 5 points  $s_i$  –the last 5  $s_i$ – for which  $s_i > s_0$ . This means that we are putting only 5 constraints on the asymptotics of the form factor and the remaining 20 points contribute to the sum rules constraints. This can be interpreted as follows: A successful implementation of the FESR will reproduce the low energy spectral density profile while the positive semidefinite condition of the  $B$ –Matrix requires the inequality  $|\mathcal{F}|^2 \leq \rho$  to be saturated up to some energy, and then it will stop saturating –at low energy the main contribution in the spectral density comes from inserting 2–particle pion states while at large energy multiparticle states start contributing–. There are many asymptotic profiles that the spectral density can attend that match the low energy spectral density profile, however, due to the saturation of the inequality with 2–particle states,  $|\mathcal{F}|^2 \sim \rho$ , the form factor asymptotics “squeeze” the profile to a low energy peak of the spectral density. Convergence at  $M = 25$  therefore means that it is enough to set 5 points, just above  $s_0$  and far beyond  $s_0$ , to set  $\rho$  with the right asymptotics. Notice that at  $M = 121$  few points are missing. This is due to the weak unfeasibility of the optimization problem and therefore, a different tuning of the regularization  $M_{Reg} = 1000$  is needed, see [1] for details. From now on we consider  $M < 100$  so that  $M_{Reg}$  does not need further tuning.

Similarly, the constraints on  $l_{max}$  and  $n_{max}$  are tested in Figures 6 and 8 for  $M = 49$  and  $M = 25$  respectively. We observe that after constraining 7 non-trivial (recall even isospin partial waves have only non-zero amplitude for even angular momentum and similarly for odd isospin waves with odd angular momentum) partial waves, the space reaches a stable position where high precision computations require few constraints more.

Likewise, for fixed  $l_{max} = 7$ , according to the Figure 8, we should expect a stabilization after  $n_{max} > 29$ . This is indeed verified with the phase shifts  $\delta_\ell^I$  for the  $S0$ ,  $P1$  and  $D0$ , plotted in Figure 7, where after  $n_{max} > 28$  the amplitude reaches a stable point in which higher contributions finely tune the amplitudes until a point where the highly oscillatory character of the basis  $\phi_n$  interferes with the high precision. On the plot we also see good agreement with experiment and phenomenological models, in orange dots and black lines respectively. We leave the comments of this for the next section where the best parameters are chosen.

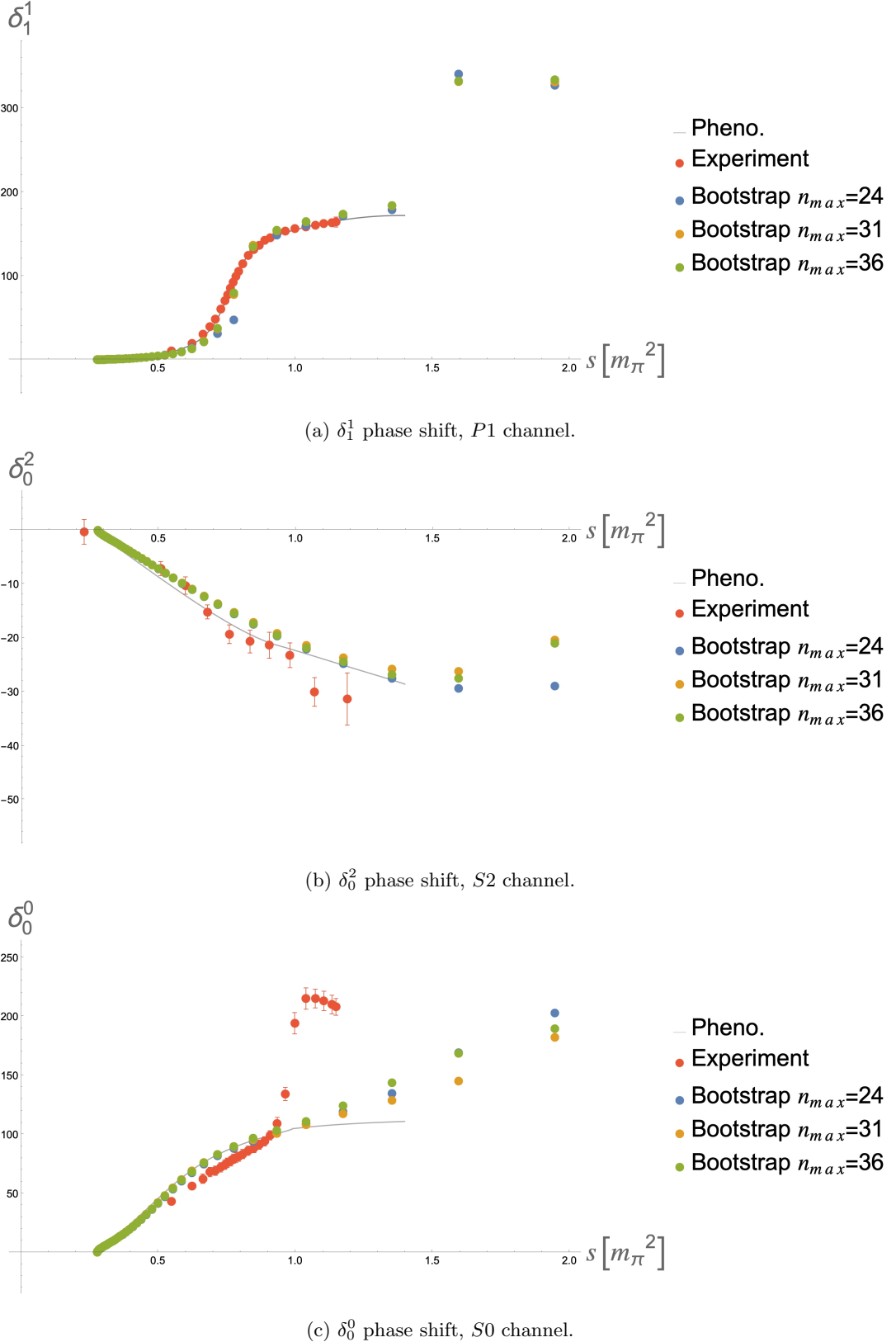


FIG. 7: Phase shift  $\delta_\ell^I$ . The convergence on the  $n_{max}$  parameter is tested for fixed  $M$  and  $l_{max}$ .

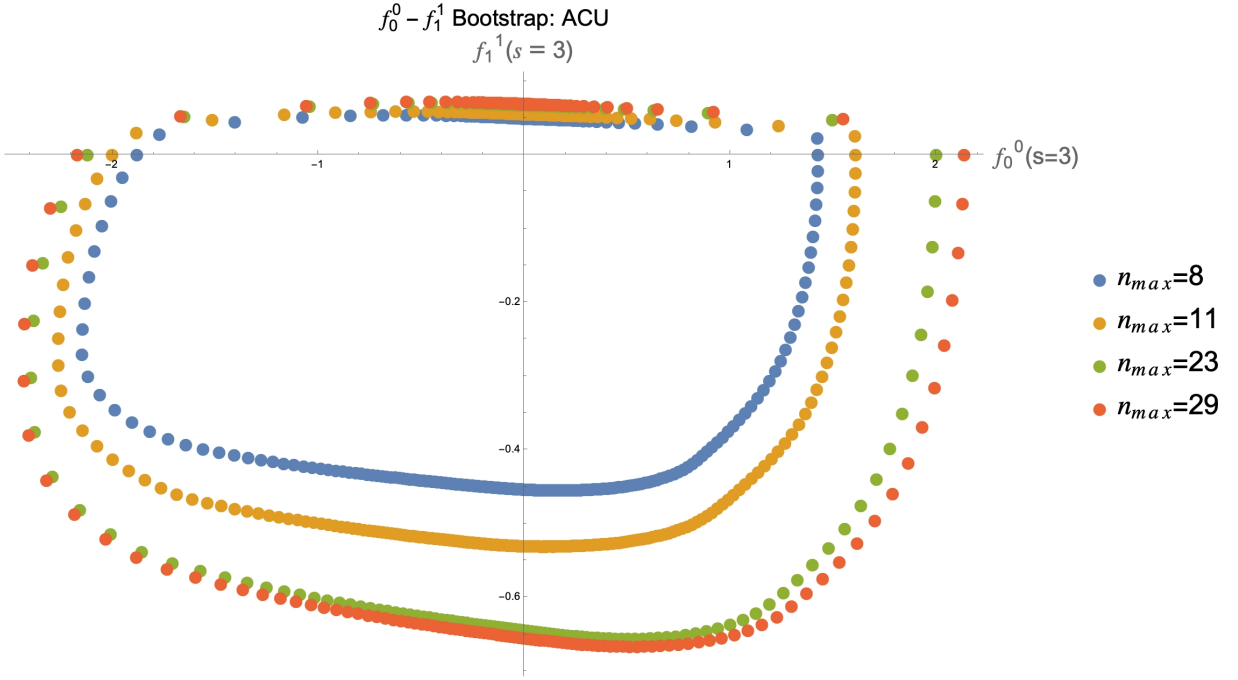


FIG. 8:  $n_{max}$  convergence comparison.  $M = 25$ ,  $l_{max} = 7$ .

### A. Results

The numerical convergence allows us to choose a set of parameters that best stabilizes the bootstrap and optimizes the method. Being conservative, we choose  $M = 49$ ,  $n_{max} = 31$  and  $l_{max} = 11$  which improves the optimization problem from roughly 30 minutes to 2 on an ordinary computer while keeping the same information found in [3] using the same order of magnitude in the tolerance parameters  $\varepsilon_{CSB}$ ,  $\varepsilon_{SVZ}$  and  $\varepsilon_{FF}$  to be

$$\varepsilon_{CSB} = 2 \times 10^{-3}, \quad \varepsilon_{FF0} = 3 \times 10^{-8}, \quad \varepsilon_{SVZ0} = 1 \times 10^{-7}, \quad (28)$$

$$M_{Reg} = 1000, \quad \varepsilon_{FF1} = 2 \times 10^{-6}, \quad \varepsilon_{SVZ1} = 4 \times 10^{-6}. \quad (29)$$

$$\varepsilon_{FF2} = 2 \times 10^{-6}, \quad \varepsilon_{SVZ2} = 4 \times 10^{-6}, \quad (30)$$

where  $\varepsilon_{FFi}$  and  $\varepsilon_{SVZi}$ ,  $i = 0, 1, 2$ , refers to the constraints on the form factors  $\mathcal{F}(s)$  and spectral densities  $\rho(s)$  (not to be confused with the bootstrap variable  $\rho_\alpha$ ) of the  $S0$ ,  $P1$  and  $D0$  partial waves.

Following [3], the results can be compared from experiments [4] and from phenomenological fits [5] where the phase shift,  $\delta_\ell^I$  are shown in Figure 9. Notice that the experimental data in the  $S0$  channel includes Kaon production leading to a rise of the phase shift around 1 GeV which we do not expect to reproduce as we are not considering the strange quark. Therefore, the phenomenological fit plot of Figure 9 is done using the parametrization with the Kaon production removed, in which case it considerably agree with the bootstrap phase shift. Figure 9a indicates a wide rise at  $\sqrt{s} \sim 200 - 800\text{MeV}$  that suggest an identification of the  $\sigma$  meson while the rise on the  $P1$  channel of Figure 9c, at  $\sqrt{s} \sim 800\text{MeV}$ , indicates the  $\rho(770)$  meson and, moreover, it shows another phase rise at  $\sqrt{s} \sim 1.6\text{GeV}$  corresponding to another resonance which should be identified with  $\rho(1450)$ . Finally, we observe a rise in the  $D0$  channel of Figure 9e indicating the  $f_2(1270)$  meson resonance. All of these were further identified in the plot of the poles of the  $T$ -Matrix showed in Figure 9g and explained below.

Figure 9g shows the poles for the  $S$ -matrix (recall  $M_\pi = 1$ ). Here we have evaluated the coefficients  $A$  and  $B$  of (12) on the grid  $[0, 1000] \times [0, 1000]$  of the real and imaginary parts of  $\sqrt{s}$  i.e.  $(Re[\sqrt{s}], Im[\sqrt{s}]) \in [0, 1000] \times [0, 1000]$ , with a resolution of 0.4 and, we have used the bootstrapped parameters of Figure 9. Remarkably, Figure 9g allow us to identify, in addition to the results of [3], the  $\sigma$  a.k.a the  $f_0(550)$  meson within the range of the PDG group [7], showed in yellow on the left hand side plot, and the  $\rho(770)$  meson with a distance error of 7% to the PDG value [7], showed on the right hand side plot by a yellow point. These novel results were difficult to find employing the methods of [3] as the  $T$ -Matrix pole  $s \in \mathbb{C}$  for the  $\sigma$  meson localizes far from the real axis and thus, the interpolation point did not have enough resolution as for the map  $\nu(\varphi)$  of Equation (13),  $\nu(\varphi) = \frac{8}{1+\cos\varphi}$ , maps high energies ( $\varphi$  close to  $\pi$ ) to very far separated points.

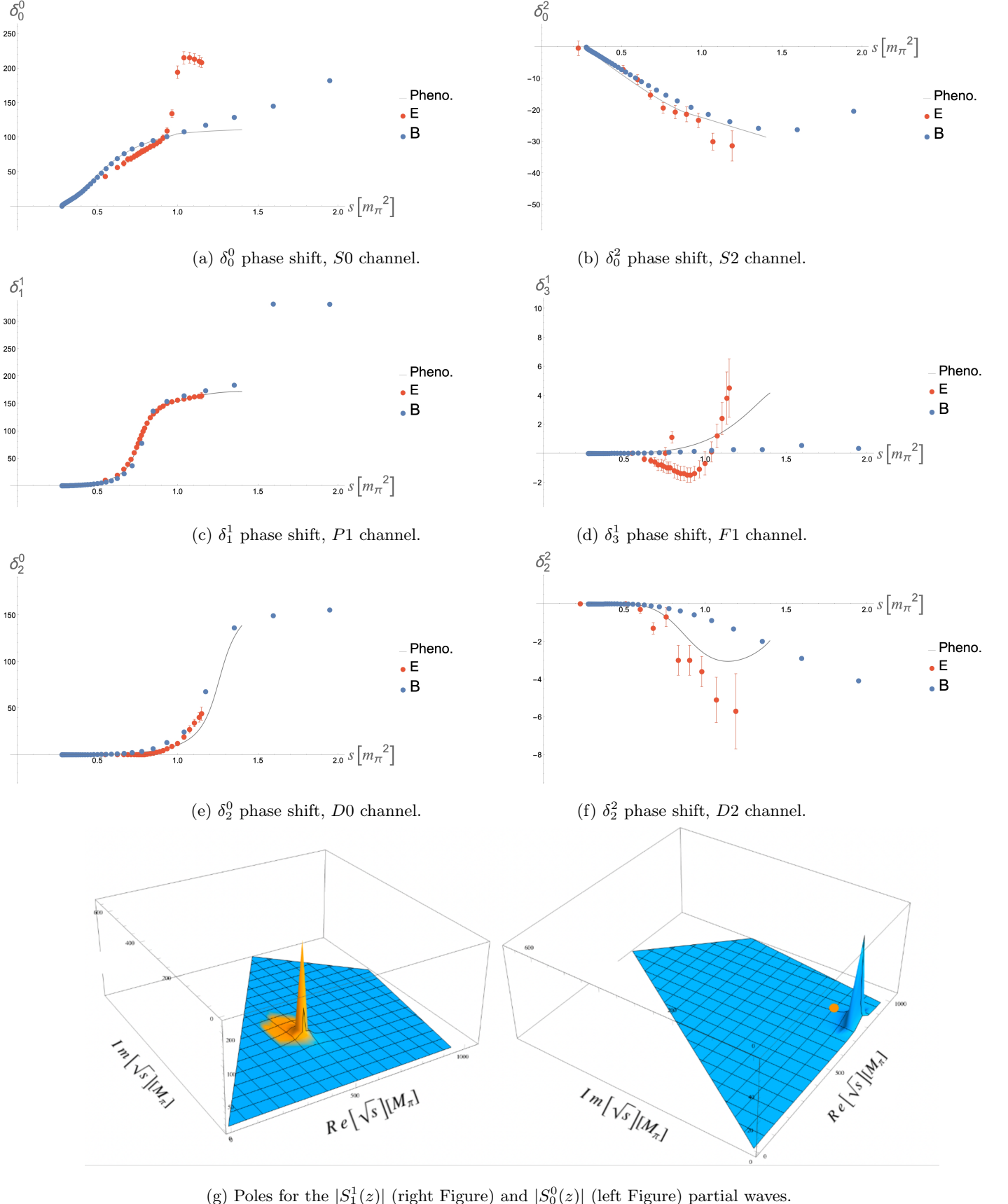


FIG. 9: First six phase shifts  $\delta_\ell^I$ . On orange are the experimental figures reported in [4], the black continuous line is the phenomenological model presented in [5] and, on blue the bootstrap result for the up extremal point. On Figure 9g the yellow zone on the left indicates where the  $\sigma$  meson is to be found, according to the PDG [7]. The yellow dot on the right indicates where the  $\rho(770)$  meson is to be found, according to the PDG [7]

## V. CONCLUSIONS

In this report we have given an introduction to the novel Gauge Theory Bootstrap initiated on [2] and further explored on [3]. This bootstrap allow us to study the strongly coupled QCD dynamics of pions at energies where the low energy effective field theory is no longer a good approximation since even at moderate energies we need a large number of couplings that we do not know how to compute from the gauge theory.

We started by imposing the general constraints of Analyticity, Crossing Symmetry and Unitarity and constrain the resulting allowed space to match the high (perturbative QCD) and low energy (Chiral perturbation theory) behavior. The boundary points are special points in this space as they constitute the amplitudes at which the scattering is dominated by 2-particle pion states and thus, where the non-perturbative results are found. We use the bootstrap as a theoretical tool to compute non-perturbative amplitudes of the 2 – 2 pion scattering. The results are promising giving great agreement with the literature although to understand the spaces of allowed amplitudes a lot of work remains to be done.

We also implemented the numerical bootstrap in the discrete basis of functions allowing to efficiently compute the dynamics of the system, reducing the generation of results considerably from 30 minutes of the previous method [3] to 2 minutes. We also check the consistency of the gauge theory bootstrap and, finally, we used that same tool to numerically identify the first resonances on the  $S_0$  and  $P_1$  partial waves, where good agreement with the theoretical and experimental predictions allow us to identify the  $\sigma$ ,  $\rho(770)$  and the  $f_2(1270)$  mesons. Overall, the new results further confirm that the Gauge Theory Bootstrap works and, it shows the advantage of using the discrete basis method for retrieving efficiently non-perturbative results.

On a more personal note, I have enjoyed my time in the LPENS team. The working environment was very good, and I am very thankful to all the members that have contributed to make it feel that way. I am specially thankful to Yifei He for his supervision and trust. I was allowed to work in a very autonomous way and the regular meetings we had were very enlightening and helpful. The experience of trying to understand deeply a physical system with bootstrap ideas has definitely sparked my interest in the field of both analytical and numerical bootstrap where great results have already been produced and many work remains to be done. I am looking forward to learning more about this field.

- [1] Y. He and M. Kruczenski, S-matrix bootstrap in 3+1 dimensions: regularization and dual convex problem, JHEP **08**, 125, arXiv:2103.11484 [hep-th].
- [2] Y. He and M. Kruczenski, Bootstrapping gauge theories, (2023), arXiv:2309.12402 [hep-th].
- [3] Y. He and M. Kruczenski, Gauge Theory Bootstrap: Pion amplitudes and low energy parameters, (2024), arXiv:2403.10772 [hep-th].
- [4] S. D. Protopopescu, M. Alston-Garnjost, A. Barbaro-Galtieri, S. M. Flatté, J. H. Friedman, T. A. Lasinski, G. R. Lynch, M. S. Rabin, and F. T. Solmitz,  $\pi\pi$  partial-wave analysis from reactions  $\pi^+p \rightarrow \pi^+\pi^-\Delta^{++}$  and  $\pi^+p \rightarrow K^+K^-\Delta^{++}$  at 7.1 gev/c, Phys. Rev. D **7**, 1279 (1973).
- [5] J. R. Peláez and F. J. Ynduráin, Pion-pion scattering amplitude, Physical Review D **71**, 10.1103/physrevd.71.074016 (2005).
- [6] J. F. Donoghue, E. Golowich, and B. R. Holstein, *Dynamics of the Standard Model*, 2nd ed., Cambridge Monographs on Particle Physics, Nuclear Physics and Cosmology (Cambridge University Press, 2014).
- [7] R. L. Workman and Others (Particle Data Group), Review of Particle Physics, PTEP **2022**, 083C01 (2022).
- [8] D. Simmons-Duffin, Tasi lectures on the conformal bootstrap (2016), arXiv:1602.07982 [hep-th].
- [9] S. Rychkov, *EPFL Lectures on Conformal Field Theory in  $D \geq 3$  Dimensions* (Springer International Publishing, 2017).
- [10] M. Kruczenski, J. Penedones, and B. C. van Rees, Snowmass white paper: S-matrix bootstrap (2022), arXiv:2203.02421 [hep-th].
- [11] M. F. Paulos, J. Penedones, J. Toledo, B. C. van Rees, and P. Vieira, The s-matrix bootstrap. part i: Qft in ads, Journal of High Energy Physics **2017**, 10.1007/jhep11(2017)133 (2017).
- [12] D. Karateev, S. Kuhn, and J. Penedones, Bootstrapping massive quantum field theories, Journal of High Energy Physics **2020**, 10.1007/jhep07(2020)035 (2020).
- [13] M. F. Paulos, J. Penedones, J. Toledo, B. C. van Rees, and P. Vieira, The s-matrix bootstrap ii: two dimensional amplitudes, Journal of High Energy Physics **2017**, 10.1007/jhep11(2017)143 (2017).
- [14] M. F. Paulos, J. Penedones, J. Toledo, B. C. van Rees, and P. Vieira, The s-matrix bootstrap iii: Higher dimensional amplitudes (2017), arXiv:1708.06765 [hep-th].
- [15] J. F. Donoghue, J. Gasser, and H. Leutwyler, The decay of a light higgs boson, Nuclear Physics B **343**, 341 (1990).
- [16] S. Weinberg, A Model of Leptons, Phys. Rev. Lett. **19**, 1264 (1967).
- [17] K. G. Wilson, Confinement of Quarks, Phys. Rev. D **10**, 2445 (1974).